

The Kinematic Sunyaev-Zel'dovich Effect with Projected Fields: A Novel Probe of the Baryon Distribution with *Planck*, *WMAP*, and *WISE* Data

J. Colin Hill,^{1,*} Simone Ferraro,² Nick Battaglia,³ Jia Liu,¹ and David N. Spergel³

¹*Dept. of Astronomy, Pupin Hall, Columbia University, New York, NY USA 10027*

²*Miller Institute for Basic Research in Science, University of California, Berkeley, CA, 94720, USA*

³*Dept. of Astrophysical Sciences, Peyton Hall, Princeton University, Princeton, NJ USA 08544*

The kinematic Sunyaev-Zel'dovich (kSZ) effect — the Doppler boosting of cosmic microwave background (CMB) photons due to Compton-scattering off free electrons with non-zero bulk velocity — is an ideal tool to probe the abundance and distribution of baryons in the Universe. All kSZ measurements to date have explicitly required spectroscopic redshifts. Here, we implement a novel estimator for the kSZ – large-scale structure cross-correlation based on projected fields: it does not require redshift estimates for any individual objects, allowing kSZ measurements from large-scale imaging surveys for the first time. We apply this estimator to cleaned CMB temperature maps constructed from *Planck* and *Wilkinson Microwave Anisotropy Probe* data and a galaxy sample from the *Wide-field Infrared Survey Explorer* (*WISE*). We measure the kSZ effect at 3.8–4.5 σ significance, depending on the use of additional *WISE* galaxy bias constraints. We verify that our measurements are robust to possible dust emission from the *WISE* galaxies. Assuming the standard Λ CDM cosmology, we directly constrain $(f_b/0.155)(f_{\text{free}}/1.0) = 1.48 \pm 0.19$ (statistical error only) at redshift $z \approx 0.4$, where f_b is the fraction of matter in baryonic form and f_{free} is the free electron fraction. This is the tightest kSZ-derived constraint reported to date on these parameters. Astronomers have long known that baryons do not trace dark matter on \sim kpc scales and there has been strong evidence that galaxies are baryon-poor. The consistency between the f_b value found here and the values inferred from analyses of the primordial CMB and Big Bang nucleosynthesis verifies that baryons approximately trace the dark matter distribution down to \sim Mpc scales. While our projected-field estimator is already competitive with other kSZ approaches when applied to current datasets (because we are able to use the full-sky *WISE* photometric survey), it will yield enormous signal-to-noise when applied to upcoming high-resolution, multi-frequency CMB surveys.

PACS numbers: 98.80.-k, 98.70.Vc

Introduction— In the standard cosmological paradigm, the primordial cosmic microwave background (CMB) anisotropies [1–3] and the abundance of light elements formed in the primordial plasma [4], known as Big Bang nucleosynthesis (BBN), imply that the baryon density (ρ_b) is approximately one-sixth of the total matter density (ρ_m): $f_b \equiv \rho_b/\rho_m = 0.155$ [3]. Yet, in galaxies, the inferred baryon/dark matter ratio is roughly a factor 2–3 lower [5, 6]. The “missing baryons” are thought to reside in an ionized, diffuse, warm-hot plasma, which has been difficult to detect in X-ray emission or absorption line studies, although recent *Hubble Space Telescope* observations indicate that many such baryons are indeed located in the circumgalactic medium of typical low-redshift galaxies ($z \approx 0.2$) [7].

In this paper, we measure the cross-correlation of the kinematic Sunyaev-Zel'dovich (kSZ) effect and the distribution of infrared-selected galaxies using a novel estimator. We infer a baryon/dark matter ratio consistent with the cosmological value: this measurement implies that most of the baryons are in ionized gas tracing the dark matter on \sim Mpc scales and above.

The kSZ effect arises from the Doppler boosting of CMB photons as they Compton-scatter off free electrons moving with a non-zero line-of-sight (LOS) velocity with respect to the CMB rest frame [8–10]. This effect leads to

a shift in the observed CMB temperature in the direction of the electrons, with an amplitude proportional to the mass in electrons and their LOS velocity, which is equally likely to be positive or negative. Since the electrons and dark matter are expected to move in the same large-scale velocity field, the kSZ signal traces the overall mass distribution, unlike the thermal Sunyaev-Zel'dovich (tSZ) effect, whose amplitude is proportional to the electron pressure and is thus primarily sourced by galaxy groups and clusters [11, 12].

The kSZ effect was first detected recently using data from the Atacama Cosmology Telescope (ACT) [13] by studying the pairwise momenta of galaxy groups and clusters (e.g., [14]). Subsequent detections using the pairwise-momentum estimator and a velocity-field reconstruction estimator [21, 22] were reported by *Planck* [23] and ACTPol [24]¹. Crucially, these estimators rely explicitly on spectroscopic data, which is much more expensive and time-consuming to acquire than photometric imaging data. Even excellent photometric redshifts lead to significantly decreased signal-to-noise (S/N) for these estimators, compared to spectroscopic data [25, 26].

¹ A high-resolution analysis of an individual galaxy cluster also found evidence for the kSZ effect in that system [15, 16].

Here, we implement a kSZ estimator based on projected fields: it can be applied to any large-scale structure sample, including galaxies, quasars, or gravitational lensing maps, allowing analyses of densely-sampled, full-sky surveys. First suggested in Refs. [19, 20], the estimator relies on the fact that a frequency-cleaned CMB temperature map contains kSZ information on small scales, regardless of whether external velocity information is available. The kSZ information can be accessed in cross-correlation with tracers of the large-scale density field. To avoid the cancellation of positive and negative kSZ signals (which are equally likely), we square the CMB temperature map in real space before cross-correlating.²

This kSZ²-tracer cross-correlation probes a wider range of physical scales than those accessible to the pairwise velocity method. On large scales, this method constrains f_b or f_{free} without the need for individual halo mass estimates. Here, f_{free} denotes the fraction of electrons that are not bound in neutral media, and thus take part in Compton scattering.

We measure the kSZ²-tracer cross-correlation in this Letter using data from *Planck* [27], the *Wilkinson Microwave Anisotropy Probe* (*WMAP*) [28], and the *Wide-field Infrared Survey Explorer* (*WISE*) [29]. In a companion paper [30] (hereafter F16), we provide theoretical details, compare to numerical simulations, and investigate the potential reach of this method for upcoming surveys. We assume the best-fit *Planck* + *WMAP* polarization ΛCDM cosmological parameters [3] (the final column of their Table 2).

Theory— The fractional CMB temperature shift induced by the kSZ effect, $\Theta^{\text{kSZ}}(\hat{\mathbf{n}}) \equiv \Delta T^{\text{kSZ}}(\hat{\mathbf{n}})/T_{\text{CMB}}$, in a direction $\hat{\mathbf{n}}$ on the sky is

$$\Theta^{\text{kSZ}}(\hat{\mathbf{n}}) = -\frac{1}{c} \int_0^{\eta_{\text{re}}} d\eta g(\eta) \mathbf{p}_e \cdot \hat{\mathbf{n}}, \quad (1)$$

where T_{CMB} is the mean CMB temperature, $\eta(z)$ is the comoving distance to redshift z , η_{re} is the comoving distance to the end of hydrogen reionization, $g(\eta) = e^{-\tau} d\tau/d\eta$ is the visibility function, τ is the optical depth to Thomson scattering, and $\mathbf{p}_e = (1 + \delta_e)\mathbf{v}_e$ is the electron momentum, with $\delta_e \equiv (n_e - \bar{n}_e)/\bar{n}_e$ the electron overdensity, n_e the free electron number density, and \mathbf{v}_e the electron peculiar velocity.

The projected galaxy overdensity is

$$\delta_g(\hat{\mathbf{n}}) = \int_0^{\eta_{\text{max}}} d\eta W_g(\eta) \delta_m(\eta\hat{\mathbf{n}}, \eta), \quad (2)$$

where η_{max} is the maximum comoving distance of the galaxy sample, $\delta_m \equiv (\rho_m - \bar{\rho}_m)/\bar{\rho}_m$ is the matter overdensity, ρ_m is the matter density, and $W_g(\eta) = b_g p_s(\eta)$

is the projection kernel. Here, b_g is the linear galaxy bias and $p_s(\eta)$ is the distribution of source galaxies, normalized to have unit integral.

To downweight angular scales dominated by primary CMB fluctuations and detector noise, we apply a filter F_ℓ in harmonic space [19], $F_\ell = C_\ell^{\text{kSZ}}/C_\ell^{\text{tot}}$, where C_ℓ^{kSZ} is the (theoretical) kSZ power spectrum and C_ℓ^{tot} is the total fluctuation power, which includes the primary CMB, kSZ effect, integrated Sachs-Wolfe (ISW) effect, noise, and any residual foregrounds. We use a theoretical kSZ power spectrum template derived from cosmological hydrodynamics simulations [33] and semi-analytic models [34]. Furthermore, as the CMB is observed through a finite telescope beam b_ℓ (in our case, a Gaussian with FWHM = 5 arcmin), the total filtered map is related to the true CMB anisotropy by $\Theta_f(\ell) = F_\ell b_\ell \Theta(\ell) \equiv f_\ell \Theta(\ell)$, where we have defined $f_\ell = F_\ell b_\ell$. F_ℓ is shown in F16.

Direct cross-correlation of Θ^{kSZ} and δ_g is expected to vanish due to the $\mathbf{v}_e \rightarrow -\mathbf{v}_e$ symmetry of the kSZ signal (i.e., positive or negative LOS velocities are equally likely). We thus square the filtered Θ^{kSZ} in real space before cross-correlating with δ_g [19, 20]. In the Limber approximation [35], this angular cross-power spectrum is given by

$$C_\ell^{\text{kSZ}^2 \times \delta_g} = \frac{1}{c^2} \int_0^{\eta_{\text{max}}} \frac{d\eta}{\eta^2} W_g(\eta) g^2(\eta) \mathcal{T}\left(k = \frac{\ell}{\eta}, \eta\right), \quad (3)$$

where

$$\mathcal{T}(k, \eta) = \int \frac{d^2 \mathbf{q}}{(2\pi)^2} f(q\eta) f(|\mathbf{k} + \mathbf{q}|\eta) B_{\delta p_{\hat{\mathbf{n}}}^e p_{\hat{\mathbf{n}}}^e}(\mathbf{k}, \mathbf{q}, -\mathbf{k} - \mathbf{q}). \quad (4)$$

Here, $B_{\delta p_{\hat{\mathbf{n}}}^e p_{\hat{\mathbf{n}}}^e}$ is the hybrid bispectrum of one density contrast δ and two LOS electron momenta $p_{\hat{\mathbf{n}}}^e$. Following Refs. [19, 20], we approximate $B_{\delta p_{\hat{\mathbf{n}}}^e p_{\hat{\mathbf{n}}}^e} \approx v_{\text{rms}}^2 B_m^{\text{NL}}/3$, where v_{rms}^2 is the linear-theory velocity dispersion and B_m^{NL} is the non-linear density bispectrum, for which we use a fitting function from numerical simulations [36]. We cross-check this approach with hydrodynamical simulations in F16.

The visibility function $g(\eta) \propto f_b f_{\text{free}}$, and thus $C_\ell^{\text{kSZ}^2 \times \delta_g} \propto f_b^2 f_{\text{free}}^2$, weighted by the kernels in Eq. (3). At the S/N level of our measurements, we cannot constrain the redshift dependence of these quantities, and thus simply fit an overall amplitude. We also assume that the free electrons trace the overall density field on the scales accessible to *Planck*; higher-resolution experiments can directly measure the free electron profiles around galaxies and clusters, which influence the small-scale shape of $C_\ell^{\text{kSZ}^2 \times \delta_g}$.

Since $C_\ell^{\text{kSZ}^2 \times \delta_g}$ is quadratic in the CMB temperature, this estimator receives a contribution from gravitational lensing of the CMB (e.g., [37]). We compute this term at first order in the lensing potential and cross-validate with simulations [38] in F16. The lensing contamination

² Other choices are possible, but squaring is perhaps the simplest approach.

is

$$\Delta C_{\ell, \text{lens}}^{\text{kSZ}^2 \times \delta_g} \approx -2 \int \frac{d^2 \mathbf{L}}{(2\pi)^2} \left\{ f(L) f(|\mathbf{L} - \boldsymbol{\ell}|) \boldsymbol{\ell} \cdot (\mathbf{L} - \boldsymbol{\ell}) \right. \\ \left. \times \left[C_{\ell}^{\psi \delta_g} C_{|\mathbf{L} - \boldsymbol{\ell}|}^{TT} + C_{\ell}^{\psi T} C_{|\mathbf{L} - \boldsymbol{\ell}|}^{T \delta_g} \right] \right\}, \quad (5)$$

where ψ is the CMB lensing potential and T is the unlensed CMB temperature. The lensing contribution is proportional to b_g . We can thus improve the $C_{\ell}^{\text{kSZ}^2 \times \delta_g}$ measurement by externally constraining b_g via cross-correlation of the *WISE* galaxies with *Planck* CMB lensing maps ($C_{\ell}^{\kappa_{\text{CMB}} \delta_g}$, where κ_{CMB} is the lensing convergence). Alternatively, the lensing contamination can be fit simultaneously with the kSZ² amplitude and marginalized over.

Data— The kSZ signal is extracted from a frequency-cleaned CMB temperature map [39]³, which we further clean using methods described below. This map is constructed from a joint analysis of the nine-year *WMAP* [28] and *Planck* full mission [27] full-sky temperature maps. The CMB is separated from other components in the microwave sky using “local-generalized morphological component analysis” (LGMCA), a technique relying on the sparse distribution of non-CMB foregrounds in the wavelet domain [31, 32]. The method reconstructs a full-sky CMB map with minimal dust contamination. Importantly for our purposes, the tSZ signal is explicitly projected out in the map construction (unlike in, e.g., the *Planck* SEVEM, NILC, or SMICA component-separated CMB maps [40]). Components that preserve the CMB blackbody spectrum are not removed, including the kSZ and ISW signals.

To isolate the kSZ signal in the LGMCA temperature map, we apply a filter as described above. We set $C_{\ell}^{\text{tot}} = \hat{C}_{\ell}^{\text{LGMCA}}$, where $\hat{C}_{\ell}^{\text{LGMCA}}$ is the measured power spectrum of the LGMCA map. We further set the filter to zero at $\ell \lesssim 100$ and $\ell \gtrsim 3000$ in order to remove ISW contamination and noise-dominated modes, respectively. We multiply by appropriate hyperbolic tangent functions at these boundaries to allow the filter to smoothly interpolate to zero, and normalize the filter such that its maximum value is unity, which occurs at $\ell \approx 2200$ (see F16).

We construct a galaxy sample from *WISE*, which imaged the sky in four photometric bands between 3.4 and 22 μm . We use the same color-based selection criteria as Ref. [41], originally based on Ref. [42]. The redshift distribution of these galaxies was obtained in Ref. [43], with a peak around $z \approx 0.3$ and extending to $z \approx 1$ (mean $\langle z \rangle \approx 0.4$). Their luminosities are similar to that of the

Milky Way ($L \sim L^*$). We apply a conservative Galactic mask to remove stellar contamination (which would not bias our results in any case, but only add to the noise). We combine this mask with a conservative point-source mask removing all sources detected at $> 5\sigma$ in the *Planck* data (as in Ref. [44]), leaving a sky fraction $f_{\text{sky}} = 0.447$ and 46.2 million *WISE* galaxies.

We use the *Planck* CMB lensing maps to place external constraints on the *WISE* galaxy bias b_g . We consider both the 2013 [45] and 2015 maps [46].

Analysis— We apply the $C_{\ell}^{\text{kSZ}^2 \times \delta_g}$ estimator described above to the filtered LGMCA temperature map and the *WISE* galaxy density map. Although the LGMCA map already shows very little dust contamination, we explicitly remove any residual dust associated with the *WISE* galaxies by finding the value of α that nulls the cross-correlation of δ_g and $((1 + \alpha)T_{\text{LGMCA}} - \alpha T_{\text{dust}})$, where T_{dust} is a dust template constructed from a CMB-free combination of the filtered *Planck* 217 and 545 GHz maps [47]: $T_{\text{dust}} = 1.0085(T_{545} - T_{217})$. We find a best-fit $\alpha_{\text{min}} = -0.0002 \pm 0.0001$ and subsequently construct $T_{\text{clean}} = (1 + \alpha_{\text{min}})T_{\text{LGMCA}} - \alpha_{\text{min}}T_{\text{dust}}$. All results that follow are nearly identical whether we use T_{clean} , the original T_{LGMCA} , or a version of T_{clean} constructed using the *Planck* 857 GHz map as a dust template.

Our measurement of $C_{\ell}^{T_{\text{clean}}^2 \times \delta_g}$ is shown in Fig. 1. The dominant oscillatory shape is due to the CMB lensing contribution. We measure the signal in thirteen linearly-spaced multipole bins between $\ell = 300$ and $\ell = 2900$ (bin width $\Delta\ell = 200$). The lower multipole limit ensures that no ISW signal is present. We correct for the effects of the mask (which is apodized with a Gaussian taper of FWHM = 10 arcmin) using standard methods [48] (note that the beam window function is forward-modeled in the theory calculations as described above). Error bars on the cross-power spectrum are estimated in the Gaussian approximation using the measured auto-spectra of the T_{clean}^2 and δ_g maps.

We consider several null tests to ensure that our measurement is not an artifact or the result of dust contamination. We process an LGMCA noise map (T_{noise}) constructed from the half-difference of splits of the *Planck* and *WMAP* data. The resulting cross-correlation of T_{noise} with δ_g is consistent with null (probability-to-exceed $p = 0.63$), as is T_{noise}^2 with δ_g ($p = 0.27$). We can consider the cross-correlation of T_{clean} (not squared) with δ_g as a null test for the mean dust contamination (top panel of Fig. 2). The result is consistent with null ($p = 0.19$). Note that the original T_{LGMCA} map also passes this test with $p = 0.07$, indicating that it is already dust-cleaned, though not as thoroughly as T_{clean} .

The most stringent dust null test is a cross-correlation of $(T_{\text{clean}}T_{\text{dust}})$ with δ_g (bottom panel of Fig. 2). In our main analysis, we cross-correlate T_{clean}^2 with δ_g , while here we replace one factor of T_{clean} with a strong

³ http://www.cosmostat.org/research/cmb/planck_wpr2

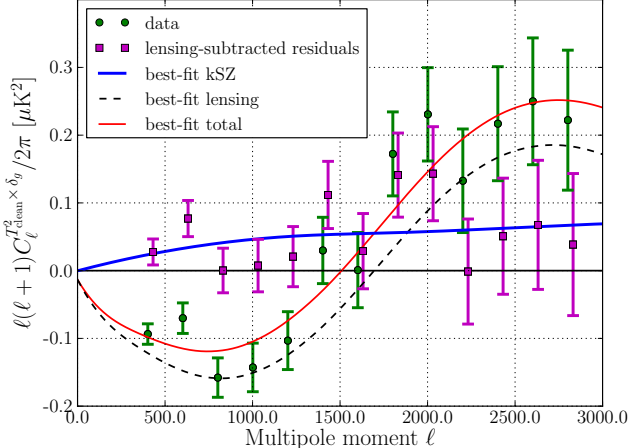


FIG. 1: Cross-power spectrum of filtered, squared T_{clean} map with *WISE* galaxies (green circles). The thick blue, dashed black, and thin red curves show the best-fit kSZ, CMB lensing, and kSZ + lensing power spectra, respectively. The kSZ signal is detected at 3.8σ significance. No external galaxy bias constraint is used in these fits; including a prior from cross-correlating the *WISE* galaxies with *Planck* CMB lensing maps produces nearly identical best-fit results (see Table I), with a kSZ significance of $4\text{--}4.5\sigma$. For visual purposes only, the magenta squares show the residual excess left after subtracting the best-fit lensing template from the data points.

dust tracer. If a significant amount of *WISE*-galaxy-correlated dust is present in T_{clean} , we should see a strong signal in this null test. The result is consistent with null ($p = 0.02$). Furthermore, rescaling the measured amplitude using a standard dust greybody spectrum from 545 GHz (the T_{dust} template frequency) to the CMB channels that dominate T_{LGMCA} (and T_{clean}) at $\approx 100\text{--}217$ GHz indicates that the dust contribution to the data points in Fig. 1 is $\lesssim 0.003 \mu\text{K}^2$.

To further test possible dust leakage due to fluctuating spectral indices amongst the *WISE* galaxies (which might not be fully removed in T_{clean}), we construct simulations in which each galaxy is assigned a greybody spectrum with index β drawn from a Gaussian of mean 1.75 and standard deviation 0.06 (values from [49]). The dust temperature is assumed to be 20 K and the amplitude is set by stacking the 857 GHz map at the location of the *WISE* galaxies (likely an overestimate, since Galactic dust is also present in this map). We then generate pairs of maps at various *Planck* frequencies and construct the linear combination that cancels the mean greybody spectrum and preserves the CMB blackbody spectrum. Processing these residual maps through our pipeline, we find cross-correlations with δ_g that are $\gtrsim 100$ times smaller than the measured $C_\ell^{T_{\text{clean}} \times \delta_g}$ signal. These tests establish that any dust leakage in our kSZ 2 –*WISE*

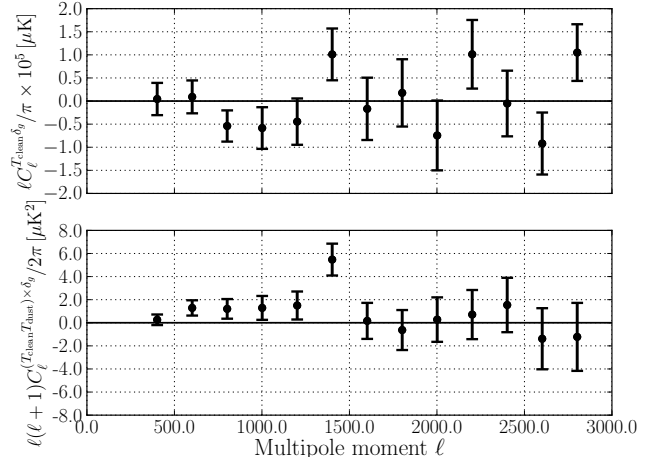


FIG. 2: Dust null tests. *Top*: Cross-correlation of T_{clean} with *WISE* galaxies. This verifies that any mean emission (e.g., dust or tSZ) of the galaxies is removed in T_{clean} . *Bottom*: Cross-correlation of $(T_{\text{clean}} T_{\text{dust}})$ with *WISE* galaxies. This verifies that any *WISE*-galaxy-correlated dust emission (including fluctuations) in T_{clean} is sufficiently removed. Rescaling T_{dust} from 545 GHz to 100–217 GHz (a factor of $\approx 400\text{--}500$) yields a dust contribution to the data points in Fig. 1 of $\lesssim 0.003 \mu\text{K}^2$, well below the statistical errors.

cross-correlation is significantly below the statistical errors of our measurement.

Finally, we consider different Galactic sky cuts, LGMCA maps from the 2013 *Planck* data, and LGMCA maps with no *WMAP* data, finding results consistent in all cases with our fiducial analysis.

As an optimization and consistency test of the separation of the CMB lensing and kSZ 2 signals in Fig. 1, we externally constrain the *WISE* galaxy bias by cross-correlating with *Planck* CMB lensing maps. Obtaining compatible values of b_g from $C_\ell^{T_{\text{clean}} \times \delta_g}$ and $C_\ell^{\kappa_{\text{CMB}} \delta_g}$ provides a strong test of our approach. We measure $C_\ell^{\kappa_{\text{CMB}} \delta_g}$ in 18 linearly spaced bins over $100 < \ell < 1900$. We estimate full covariance matrices using 100 *Planck* CMB lensing simulations (separately for the 2013 and 2015 analyses). Fitting the 2015 measurement to a theoretical model based on the most recent “halofit” prescription for the non-linear matter power spectrum [50], we find $b_g = 1.13 \pm 0.02$. We obtain consistent results with the 2013 lensing map (see also [41]) or if we restrict to $100 < \ell < 400$, where theoretical uncertainties due to nonlinearity are significantly diminished.

Interpretation— We fit a theoretical model consisting of the sum of the $C_\ell^{\text{kSZ}^2 \times \delta_g}$ prediction in Eq. (3) and the lensing contribution $\Delta C_{\ell, \text{lens}}^{\text{kSZ}^2 \times \delta_g}$ in Eq. (5), each with a free amplitude. The amplitude of the lensing contribution is simply b_g , while the amplitude of the kSZ 2 template is $\mathcal{A}_{\text{kSZ}^2} b_g$, with $\mathcal{A}_{\text{kSZ}^2} = 1$ corresponding to our

fiducial model. We simultaneously fit for $\mathcal{A}_{\text{kSZ}^2}$ and b_g assuming a Gaussian likelihood for the data. We consider three analysis scenarios (see Table I). Initially, we determine $\mathcal{A}_{\text{kSZ}^2}$ and b_g using only $C_\ell^{T_{\text{clean}}^2 \times \delta_g}$. Due to the different shapes of the theoretical templates (see Fig. 1), both amplitudes can be robustly measured. The kSZ^2 and lensing signals are detected at 3.8σ and 10σ , respectively. The kSZ^2 S/N is only slightly decreased by marginalizing over b_g ; if b_g were perfectly known, the kSZ^2 significance would be 4.3σ . The best-fit model describes the data well, with $\chi^2 = 13.1$ for 11 degrees of freedom ($p = 0.28$).

The kSZ^2 S/N can be increased by including the external constraint on b_g from our measurement of $C_\ell^{\kappa_{\text{CMB}} \delta_g}$. Including a Gaussian prior centered on $b_g = 1.13$ with standard deviation 0.02, we find consistent results for $\mathcal{A}_{\text{kSZ}^2}$ and b_g compared to the $C_\ell^{T_{\text{clean}}^2 \times \delta_g}$ -only analysis,⁴ with the kSZ^2 S/N increased to 4.5σ . Finally, to be conservative, we consider including an additional 10% theoretical systematic error on the external b_g prior, due to uncertainties in modeling κ_{CMB} and galaxy bias on small scales. In this case, we detect $\mathcal{A}_{\text{kSZ}^2}$ at 4.2σ significance.

Using $\mathcal{A}_{\text{kSZ}^2} \propto f_b^2 f_{\text{free}}^2$, our result for the $C_\ell^{T_{\text{clean}}^2 \times \delta_g}$ -only analysis yields $(f_b/0.155)(f_{\text{free}}/1.0) = 1.48 \pm 0.19$ at $z \approx 0.4$. At this redshift, hydrogen and helium are fully ionized, and thus we expect $f_{\text{free}} \approx 1$, with a small fraction of electrons bound in neutral media (e.g., stars or neutral hydrogen gas). Therefore, our measurement of f_b is consistent with the predicted abundance of baryons from the primordial CMB and BBN. This is the tightest kSZ -derived constraint on f_b presented to date.

While our value of $\mathcal{A}_{\text{kSZ}^2}$ is slightly high, additional theoretical systematic uncertainties must be accounted for in the interpretation (although these do not affect the detection significance). The amplitude of $C_\ell^{\text{kSZ}^2 \times \delta_g} \propto \sigma_8^7$ [19], where σ_8 is the matter power spectrum amplitude, and thus a change in σ_8 within current experimental limits can affect our result at the $\approx 10\%$ level. Also, there are theoretical uncertainties due to our extrapolation of the B_m^{NL} fitting function [36] to high wavenumbers where it was not explicitly calibrated, and also due to our use of linear theory for calculating v_{rms}^2 . In addition, the lensing contamination template is subject to uncertainties at high- ℓ due to nonlinear evolution and baryonic physics. However, our comparison to simulations in F16 indicates that the approximations made in our analysis are accurate.

Outlook— Our detection confirms that the expected abundance of baryons is present in the low-redshift Uni-

analysis scenario	$\mathcal{A}_{\text{kSZ}^2}$	b_g
$C_\ell^{T_{\text{clean}}^2 \times \delta_g}$ only	2.18 ± 0.57	1.10 ± 0.11
$C_\ell^{T_{\text{clean}}^2 \times \delta_g}$ and $C_\ell^{\kappa_{\text{CMB}} \delta_g}$	2.24 ± 0.50	1.13 ± 0.02
+10% theory error on $C_\ell^{\kappa_{\text{CMB}} \delta_g}$	2.21 ± 0.53	1.11 ± 0.08

TABLE I: Fits to the kSZ^2 -*WISE* galaxies cross-correlation for three analysis scenarios: (i) using only the $C_\ell^{T_{\text{clean}}^2 \times \delta_g}$ data (green circles in Fig. 1); (ii) including an external constraint on the *WISE* galaxy bias from our measurement of $C_\ell^{\kappa_{\text{CMB}} \delta_g}$; (iii) same as (ii), but including an additional 10% theoretical systematic error on the b_g constraint from $C_\ell^{\kappa_{\text{CMB}} \delta_g}$, due to uncertainties from nonlinear evolution and baryonic physics.

verse and that their distribution traces that of the dark matter (an assumption in our model), within the statistical errors. The novel projected-field estimator implemented here allows kSZ measurements with photometric imaging surveys for the first time, covering much larger sky fractions and tracer samples than spectroscopic data. In turn, this will yield enormous S/N detections with upcoming multi-frequency CMB surveys (see F16), especially for high-resolution experiments that access the kSZ -dominated modes on small angular scales. We forecast $\gtrsim 100\sigma$ kSZ^2 -*WISE* cross-correlations using the upcoming *Advanced ACTPol* [51] and CMB-S4 surveys, contingent on the efficiency of multi-frequency foreground cleaning. These high-resolution measurements will directly probe the baryon distribution as a function of scale and redshift, and the influence of baryons on the small-scale matter power spectrum. Moreover, combining kSZ constraints with tSZ analyses will directly determine the gas temperature at the virial radius and beyond. Finally, kSZ - large-scale structure cross-correlations will be essential to isolate the high-redshift kSZ signal due to “patchy” cosmic reionization from the low-redshift kSZ signal studied here. This work is a first step toward realizing these exciting new probes of the distribution of gas and matter in our Universe.

Acknowledgments. We are grateful to Olivier Doré, Zoltan Haiman, Emmanuel Schaan, Blake Sherwin, Kendrick Smith, and Jessica Werk for useful conversations. We thank the LGMCA team for publicly releasing their CMB maps. This work was partially supported by a Junior Fellow award from the Simons Foundation to JCH. SF was supported in part by the Miller Institute for Basic Research in Science at UC Berkeley. NB acknowledges support from the Lyman Spitzer Fellowship. JL is supported by NSF grant AST-1210877. JCH, SF, and DNS acknowledge support from NSF grant AST1311756 and NASA grant NNX12AG72G. Some of the results in this paper have been derived using the HEALPix package [52]. This publication makes use of data products from the *Wide-field Infrared Survey Explorer*, which is a joint project of the University of California, Los Angeles, and the Jet Propulsion Laboratory/California Institute of Technology, funded by the National Aeronautics and Space Administra-

⁴ Note that we neglect the covariance between the b_g information contained in $C_\ell^{T_{\text{clean}}^2 \times \delta_g}$ and $C_\ell^{\kappa_{\text{CMB}} \delta_g}$, as the latter dominates the combined constraint.

tion.

-
- * Electronic address: jch@astro.columbia.edu
- [1] Spergel, D. N., Verde, L., Peiris, H. V., et al. 2003, *ApJS*, 148, 175
- [2] Hinshaw, G., Larson, D., Komatsu, E., et al. 2013, *ApJS*, 208, 19
- [3] Planck Collaboration, Ade, P. A. R., Aghanim, N., et al. 2014, *A&A*, 571, AA16
- [4] Steigman, G. 2007, *Annual Review of Nuclear and Particle Science*, 57, 463
- [5] Fukugita, M., Hogan, C. J., & Peebles, P. J. E. 1998, *ApJ*, 503, 518
- [6] Bregman, J. N. 2007, *ARA&A*, 45, 221
- [7] Werk, J. K., Prochaska, J. X., Tumlinson, J., et al. 2014, *ApJ*, 792, 8
- [8] Sunyaev, R. A., & Zel'dovich, Y. B. 1972, *Comments Astrophys. Space Phys.*, 4, 173
- [9] Sunyaev, R. A., & Zeldovich, I. B. 1980, *ARA&A*, 18, 537
- [10] Ostriker, J. P., & Vishniac, E. T. 1986, *ApJ*, 306, L51
- [11] Battaglia, N., Bond, J. R., Pfrommer, C., & Sievers, J. L. 2012, *ApJ*, 758, 75
- [12] Battaglia, N., Hill, J. C., & Murray, N. 2015, *ApJ*, 812, 154
- [13] Hand, N., Addison, G. E., Aubourg, E., et al. 2012, *Physical Review Letters*, 109, 041101
- [14] Ferreira, P. G., Juskiewicz, R., Feldman, H. A., Davis, M., & Jaffe, A. H. 1999, *ApJ*, 515, L1
- [15] Mroczkowski, T., Dicker, S., Sayers, J., et al. 2012, *ApJ*, 761, 47
- [16] Sayers, J., Mroczkowski, T., Zemcov, M., et al. 2013, *ApJ*, 778, 52
- [17] Kaiser, N. 1992, *ApJ*, 388, 272
- [18] Bartelmann, M., & Schneider, P. 2001, *Phys. Rep.*, 340, 291
- [19] Doré, O., Hennawi, J. F., & Spergel, D. N. 2004, *ApJ*, 606, 46
- [20] DeDeo, S., Spergel, D. N., & Trac, H. 2005, *arXiv:astro-ph/0511060*
- [21] Ho, S., Dedeo, S., & Spergel, D. 2009, *arXiv:0903.2845*
- [22] Li, M., Angulo, R. E., White, S. D. M., & Jasche, J. 2014, *MNRAS*, 443, 2311
- [23] Planck Collaboration, Ade, P. A. R., Aghanim, N., et al. 2016, *A&A*, 586, A140
- [24] Schaan, E., Ferraro, S., Vargas-Magaña, M., et al. 2015, *arXiv:1510.06442*
- [25] Keisler, R., & Schmidt, F. 2013, *ApJ*, 765, L32
- [26] Flender, S., Bleem, L., Finkel, H., et al. 2015, *arXiv:1511.02843*
- [27] Planck Collaboration, Adam, R., Ade, P. A. R., et al. 2015, *arXiv:1502.01582*
- [28] Bennett, C. L., Larson, D., Weiland, J. L., et al. 2013, *ApJS*, 208, 20
- [29] Wright, E. L., Eisenhardt, P. R. M., Mainzer, A. K., et al. 2010, *AJ*, 140, 1868-1881
- [30] Ferraro, S., Hill, J. C., Battaglia, N., Liu, J., & Spergel, D. N. 2016, to appear
- [31] Bobin, J., Starck, J.-L., Sureau, F., & Basak, S. 2013, *A&A*, 550, A73
- [32] Bobin, J., Sureau, F., Starck, J.-L., Rassat, A., & Paykari, P. 2014, *A&A*, 563, A105
- [33] Battaglia, N., Bond, J. R., Pfrommer, C., Sievers, J. L., & Sijacki, D. 2010, *ApJ*, 725, 91
- [34] Battaglia, N., Natarajan, A., Trac, H., Cen, R., & Loeb, A. 2013, *ApJ*, 776, 83
- [35] Limber, D. N. 1953, *ApJ*, 117, 134
- [36] Gil-Marín, H., Wagner, C., Fragkoudi, F., Jimenez, R., & Verde, L. 2012, *J. Cosmology Astropart. Phys.*, 2, 047
- [37] Lewis, A., & Challinor, A. 2006, *Phys. Rep.*, 429, 1
- [38] Sehgal, N., Bode, P., Das, S., et al. 2010, *ApJ*, 709, 920
- [39] Bobin, J., Sureau, F., & Starck, J. 2015, *arXiv:1511.08690*
- [40] Planck Collaboration, Adam, R., Ade, P. A. R., et al. 2015, *arXiv:1502.05956*
- [41] Ferraro, S., Sherwin, B. D., & Spergel, D. N. 2014, *arXiv:1401.1193*
- [42] Jarrett, T. H., Cohen, M., Masci, F., et al. 2011, *ApJ*, 735, 112
- [43] Yan, L., Donoso, E., Tsai, C.-W., et al. 2013, *AJ*, 145, 55
- [44] Hill, J. C., & Spergel, D. N. 2014, *J. Cosmology Astropart. Phys.*, 2, 30
- [45] Planck Collaboration, Ade, P. A. R., Aghanim, N., et al. 2014, *A&A*, 571, A17
- [46] Planck Collaboration, Ade, P. A. R., Aghanim, N., et al. 2015, *arXiv:1502.01591*
- [47] Spergel, D. N., Flauger, R., & Hložek, R. 2015, *Phys. Rev. D*, 91, 023518
- [48] Hivon, E., Górski, K. M., Netterfield, C. B., et al. 2002, *ApJ*, 567, 2
- [49] Planck Collaboration, Ade, P. A. R., Aghanim, N., et al. 2014, *A&A*, 571, A30
- [50] Takahashi, R., Sato, M., Nishimichi, T., Taruya, A., & Oguri, M. 2012, *ApJ*, 761, 152
- [51] Henderson, S. W., Allison, R., Austermann, J., et al. 2015, *arXiv:1510.02809*
- [52] Górski, K. M., Hivon, E., Banday, A. J., et al. 2005, *ApJ*, 622, 759